Applied Physics A (2022) 128:371
https://doi.org/10.1007/s00339-022-05487-z

Applied Physics A
Materials Science & Processing

Tracking on crystallization process of doped metal oxide IATO to optimize solvothermal conditions

Te Hu[1] · Ian R. Baxendale[2] · Yuchang Su[3] · Fangjiang Li[1] · Shaomi Duan[4] · Yaping Zhang[5] · Honxin Fan[5]

Received: 13 October 2021 / Accepted: 10 March 2022

Abstract
XRD (X-ray diffraction) pattern analysis can estimate approximate preparation condition values based on nanomaterials formation; however, these initial values can be further refined without additional experiments by combining DSC (Differential Scanning Calorimetry) curves with thermodynamic equations to track crystallinity and crystallization rate of nanomaterials, which effectively improves the speed of preparation scheme. In this study, XRD pattern analysis from the comparative experimental results revealed that the optimum preparing solvothermal conditions on the IATO (tin-doped indium oxide) are at 200 °C for 24 h with 20 vol% 1-butanol; however, these conditions can be further optimized as 160 °C for 20 h with 5 vol% 1-butanol by simulating the growth process of nanomaterials in accordance to combine DSC curves with thermodynamic equations.

Keywords Solvothermal condition · Crystallinity · Crystallization rate · DSC · Thermodynamic equation · Doped metal oxide

1 Introduction

Nanometer characteristics of nanomaterials including size, morphology, agglomeration, and crystallographic structure affect the distribution of carrier concentration, the frequency of surface plasma oscillation, and the formation of small polarons thereby determining they possess distinctive physical and chemical properties.

Gao et al. [1] regulated nanostructure growth under altering solvothermal conditions to synthesize tungsten oxide as spindle-like particles, nanotubes, plate-like particles, nanowires, and nanospheres, and observed that the tungsten oxide as nanotubes with a diameter of less than 50 nm demonstrated the highest visible light transmittance and the strongest absorption of NIR light compared to other samples. Tang et al. [2] based on the solvothermal treatment of Ce(OH)CO_3 precursors with alkali solution in an aqueous phase and obtained CeO_2 well-shaped hollow nanotubes, which have obvious degradation on phenol under UV radiation. Teng et al. [3] investigated the effect of morphology on catalytic activity by applying a solvothermal system to synthesize Co_3O_4 nanocrystals of different shapes plate-like (P–Co_3O_4), rod-like (R–Co_3O_4), cubic (C–Co_3O_4), and approximately spherical (S–Co_3O_4). The best catalytic result was achieved in CO oxidation plate-like Co_3O_4 primarily exposing planes. Chai et al. [4] prepared cuprous oxide (Cu2O) microcrystals with distinct morphologies under mild solvothermal conditions, holding at 60 °C for 6 h. They explored the essence of Cu2O microcrystals adsorption and photocatalysis that six hollow branches microcrystals have higher degradation efficiency to methyl orange (MO) by connecting with cubic and truncated octahedral microcrystals. Zhang et al. [5] designed a microwave-assisted solvothermal route to synthesize MnO_2

✉ Te Hu
hutete@kust.edu.cn

1 Faculty of Science, Kunming University of Science and Technology, South Jingming Road, Kunming 650500, China

2 Department of Chemistry, Durham University, South Road, Durham DH1 3LE, United Kingdom

3 School of Materials Science and Engineering, Central South University, South Lushan Road, Changsha 410083, China

4 Faculty of Information Engineering and Automation, Kunming University of Science and Technology, South Jingming Road, Kunming 650500, China

5 Yunnan Provincial Key Laboratory of Modern Information Optics, Kunming University of Science and Technology, South Jingming Road, Kunming 650500, China

Published online: 04 April 2022

nanocrystals with 4 structures and morphologies including δ-MnO_2 microspheres, α-MnO_2 nanorods, γ-MnO_2 nanosheets, and β-MnO_2 octahedrons by reducing potassium permanganate with varying amounts of hydrochloric acid. The relevant research results showed that α-MnO_2 nanorods have the best catalytic action on redox reactions for their crystal phase/morphology by oxygen adsorption mechanism.

Depending on the results of the above research, it is found that functional nanoscale metal oxides have a certain composition of superficial carrier concentration [6–10]; therefore, they have particular properties, such as transmittance in the visible range, absorbability in IR or UV spectrum, photoelectron, oxidation, photocatalysis [11–15], which can be rationally interpreted by surface plasmon resonance theory [16, 17] that incident light as electromagnetic waves are captured on the surface of metal oxides to be resonated with external free electrons.

In addition, it is essential that the preparation conditions of nanomaterials decide their nanoscale features as well as physical and chemical properties. Hence we utilize solvothermal reaction to synthesize antimony–tin-doped indium oxide (IATO) as an example, using XRD analysis determines the effect of each solvothermal condition on sample preparation to get possible condition values, then combining DSC curve with thermodynamic equations to track the process of crystal growth of nanomaterials and to obtain crystallinity and crystallization rate will make these potential values more accurate to diminish experimental quantities and costs.

2 Experimental

Indium chloride ($InCl_3$), tin (IV) chloride pentahydrate ($SnCl_4 \bullet 5H_2O$) and antimony chloride ($SbCl_3$) with molar ratio $[In^{3+}]/[Sn^{4+}]/[Sb^{3+}] = 1/20/20$ and urea with molar ratio $[In^{3+}]/[OH^-] = 1/6$ were dissolved in disparate mixed solvents with different proportions of deionized water (4 vol%, 5 vol% or 6 vol%) and 1-butanol (5 vol%, 15 vol%, 20 vol% or 40 vol%), meanwhile, filling remaining volume with EG (ethylene glycol).

The urea-induced formation of hydroxyl anion is described by the following reaction equations:

$$CO(NH_2)_2 + H_2O = CO_2 \uparrow + 2NH_3 \uparrow \quad (1)$$

$$NH_3 + H_2O \rightleftharpoons NH_3 \cdot H_2O \quad (2)$$

$$NH_3 \cdot H_2O \rightleftharpoons NH_4^+ + OH^- \quad (3)$$

These solid–liquid mixtures were become solution with ultrasonic oscillation for a half-hour and magnetic stirring for 1 h at ambient temperature, then poured into a Teflon-lined reactor and heated at various reaction temperatures (160 °C, 180 °C or 200 °C) for individual reaction times (6 h, 18 h, 24 h or 48 h).

Colloidal products were collected in deionized water through centrifugal separation, ultrasonic dispersion, and magnetic stirring, with corresponding colors being blue–gray or green–gray solids. To indicate whether chloride ions on the surface of the collections were removed or not silver nitrate solution was employed. The products were dried in a vacuum oven at 200 °C below 0 Pa for 6 h then were ground into fine powder with an agate mortar. The crystalline phases of IATO products were characterized using XRD (Xray diffraction) on the Rigaku D/Max 2500 inspection equipment (Japan). Crystallinity and crystalline rate of IATO nanoparticles were analyzed on TG–DSC (Thermogravimetric–differential scanning calorimetry) from Netzsch (STA-449C) (Germany).

3 Results and discussion

For acquiring effect of solvothermal conditions and compositions of mixed solvent on crystal growth process of IATO nanoparticles, XRD patterns and DSC curves were adopted to evaluate the products synthesis. Table 1 shows ICDD cards of In_2O_3, $In(OH)_3$, and InOOH in XRD patterns:

Figure 1 demonstrates a change of crystallization phases of synthesized products at certain solvothermal temperatures [18–20] (160, 180 and 200 °C) for 24 h with various deionized water proportions [19, 20] (4, 5 and 6 vol%).

Figure 1a shows diverse products had been obtained using different contents of deionized water at 160 ℃ for 24 h. When 4 vol% deionized water was hired, mixture comprises cubic In_2O_3, cubic $In(OH)_3$ and orthorhombic InOOH. if content of deionized water was extended to 6 vol%, nothing but cubic $In(OH)_3$ and orthorhombic InOOH were found; however, only cubic In_2O_3 was synthesized when 5 vol% deionized water was employed.

The temperature was raised to 180 °C, cubic $In(OH)_3$ and orthorhombic InOOH were thoroughly converted into cubic In_2O_3 when 4 vol% deionized water was selected, but hiring 6 vol% deionized water they were partly transformed into cubic In_2O_3, as same with the above, taking 5 vol% deionized water cubic In_2O_3 was still single product in Fig. 1b.

Table 1 Corresponding ICDD cards of each element of solvothermal products

Elements	Crystal patterns	ICDD cards
In_2O_3	Cubic	PDF#71-2194
$In(OH)_3$	Cubic	PDF#85-1338
InOOH	Orthorhombic	PDF#73-1592

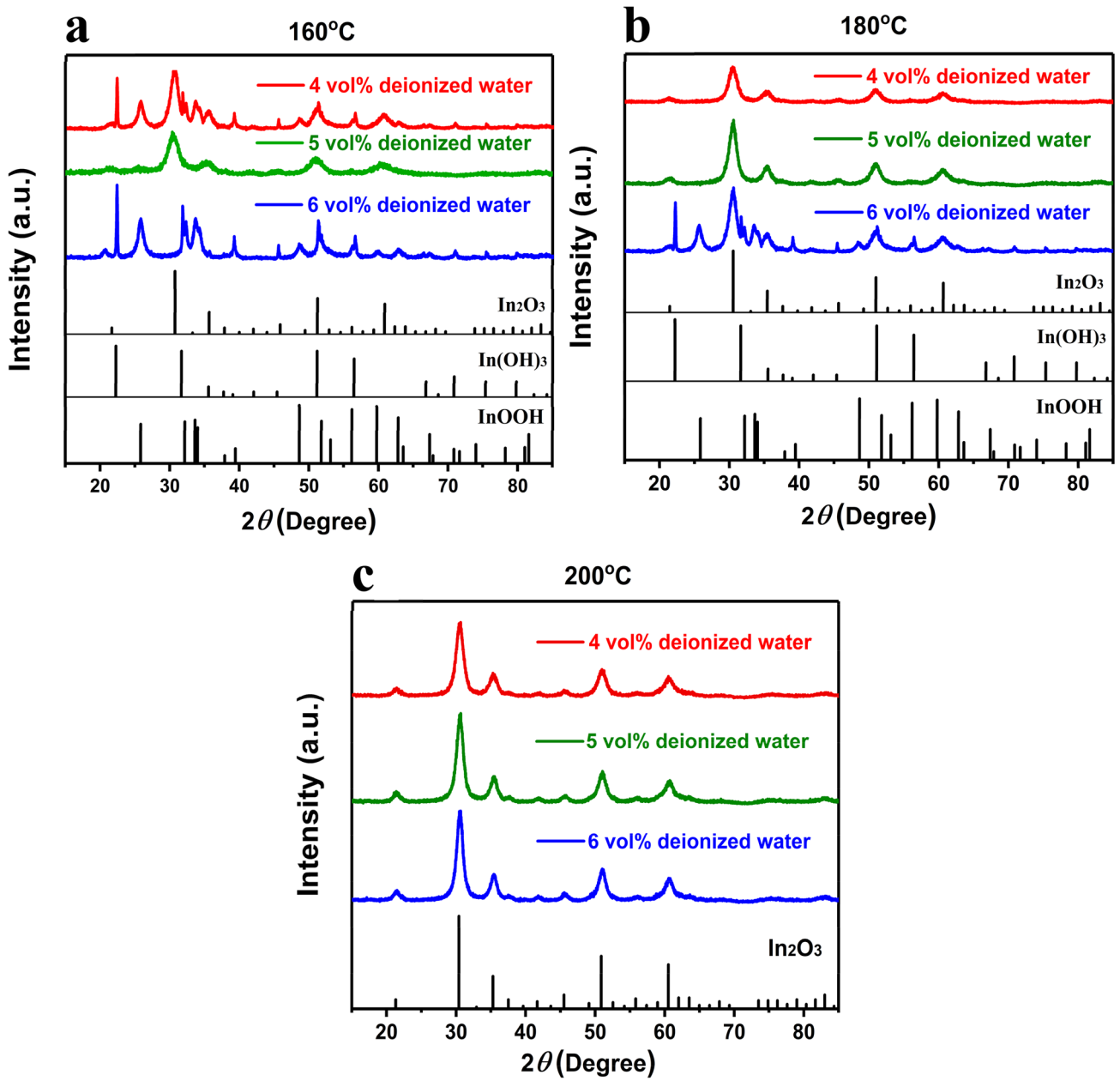

Fig. 1 Crystalline phases of IATO nanoparticles prepared at diverse solvothermal temperatures **a** 160 °C, **b** 180 °C and **c** 200 °C for 24 h with a group of contents of deionized water 4, 5 and 6 vol%

It was concluded from the results obtained at 160 and 180 ℃, it was inferred that cubic $In(OH)_3$ and orthorhombic InOOH were intended to transform into cubic In_2O_3 at higher temperatures.

As previously assumed, when solvothermal temperature was increased to 200 ℃, product was only cubic In_2O_3, whether 4 vol%, 5 vol% or 6 vol% deionized water was chosen.

Based on the above contrasting experiments, it can be deduced that optimal synthesis conditions of IATO were at 200 ℃ for 24 h, with 5 vol% deionized water and 95 vol% EG (ethylene glycol).

Figures 2, 3 illustrate XRD patterns of effects of solvothermal time [19, 20] and amount of dispersing agent [19, 21, 22] 1-butanol on the formation of IATO nanoparticles, of which, 200 ℃ and 5 vol% deionized water were invariable parameters.

Figure 2 indicates the impact of distinct reaction times on crystalline phases of IATO, using 6 and 18 h excepted for cubic In_2O_3 precursors cubic $In(OH)_3$ and orthorhombic

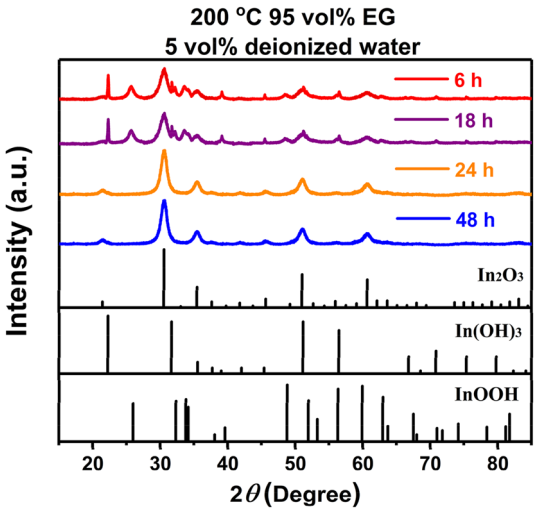

Fig. 2 Crystalline phases of IATO nanoparticles synthesized at 200 °C with 5 vol% deionized water and 95 vol% EG for diverse solvothermal times

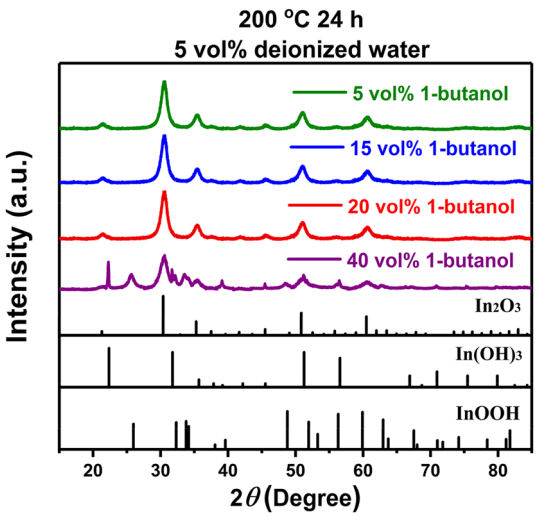

Fig. 3 Crystalline phases of IATO nanoparticles formed at 200 °C for 24 h with 5 vol% deionized water and various contents of 1-butanol

InOOH existed in final materials; however, the solvothermal time was longer than or equal to 24 h these precursors were completely transformed into cubic In_2O_3.

Function of dispersing agent 1-butanol in mixed solvent was to prevent the aggregation and reduce size of IATO nanoparticles, but when dispersing agent value reached or excessed 40 vol% intermediates cubic $In(OH)_3$ and orthorhombic InOOH cannot be turned into cubic In_2O_3 as demonstrated in Fig. 3.

Precise reaction parameter values for reducing preparation costs cannot be obtained by XRD analysis expeditiously, because the characterization method cannot record the process of crystallization to screen out the appropriate values, hence a mass of comparative experiments will be required. This gap, however, can be filled in by TG–DSC analysis to track the course of the synthetic reaction.

TG–DSC analysis results were obtained by calcine products up to 1200 °C at heating rate 10 °C/min which generate absorbed or released heat value was relevant to the section under the DSC curve. Therefore, in accordance with an exothermic or endothermic peak of the DSC curve, crystallinity $A(T_i)$ of products in the solvothermal reaction can be inferred by the proportion of between area size $S(T_i)$ under the crest temperature and total area size S(T) under the curve [23, 24]:

$$A(T_i) = \frac{S(T_i)}{S(T)} = \frac{\int_{T_0}^{T_i} f(T)dT}{\int_{T_0}^{T} f(T)dT} \tag{4}$$

$f(T) = \frac{dH}{dt}$ is heat flux.

Integral diagram of Eq. (4), as illustrated in Fig. 4

Meanwhile, crystalline rate R(t) of products in solvothermal reaction can be calculated at apex temperature by crystallinity $A(T_i)$ with time parameter t:

$$T = T_0 + \alpha t \tag{5}$$

Among, α(°C/min) is temperature rate. Differential computing on Eq. (2):

$$dT = \alpha dt \tag{6}$$

$$R(t) = \frac{dA}{dt} = \alpha \frac{dA}{dT} \tag{7}$$

Depending on these equations, crystallinity and crystallization rate of IATO nanoparticles can intuitively reflect

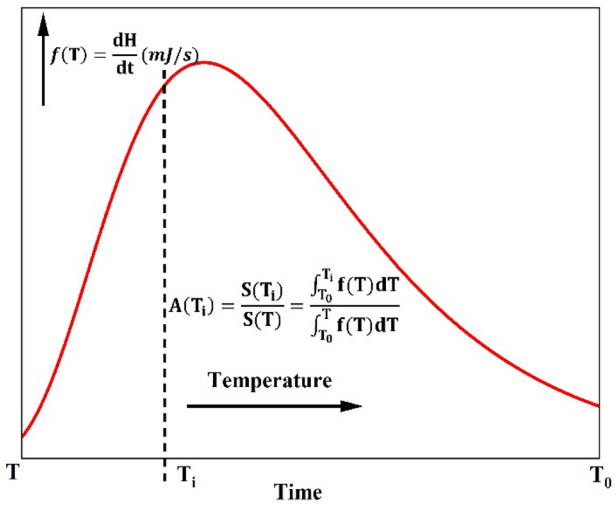

Fig. 4 Integral diagram of Eq. (1)

contributions of various solvothermal conditions on product formation, thereby selecting appropriate values to achieve synthetic process optimization.

To explore the effect of solvothermal temperature [25–27] on crystal growth, kept reaction time 24 h and 4 vol%, 5 vol%, or 6 vol% deionized water constants. Figure 5 shows exothermic peaks, crystallinity and crystalline rate on the basis of respective products DSC curves [28, 29] when solvothermal temperatures were 160 °C, 180 °C or 200 °C. Exothermic peaks are shown in Fig. 5(a1, b1, c1). All products can complete crystallinity in the three sets of solvothermal reaction conditions, as shown in Fig. 5(a2, b2, c2), particularly, the process of crystal growth in 6 vol% deionized water gradually tended to coincide with other samples as temperature rises. Correspondingly, the crystallization rate of the products was accelerated in 6 vol% deionized water as temperature increases that the required time to achieve crest value was reduced from 15 h to 12.5 h, as illustrated in Fig. 5(a3, b3, c3).

Based on these contrastive experiments, it can be observed that heading up the temperature will boost the crystallization rate of a product prepared with the higher content of deionized water then is inclined to be consistent. It is hypothesized that a high proportion of deionized water causes the specific heat capacity of the mixed solvent to increase at low temperature, thereby prolonging the process of crystalline grain growth and delaying the appearance of the crystallization rate crest. Conversely, at high temperature, the thermal force facilitates convection of the liquid phase, which dominates the entire crystal growth acceleration then making crystallization peaks from product synthesized in various deionized water contents coincide. These deductions are consistent with the changes of XRD patterns in Fig. 1 that at high-temperature the intermediates $In(OH)_3$ and InOOH can be fully converted into In_2O_3, whereas at low temperature or high content of deionized water the precursors are partially or not transformed into In_2O_3.

Solvothermal time [30] is also a crucial factor in controlling the crystallinity and crystallization rate of IATO nanoparticles, and related findings are illustrated in Fig. 6. Selecting 6, 12, 24, and 48 h participated solvothermal reaction for comparative experiments while holding on reaction temperature 200 ℃ and 5 vol% deionized water invariable. Exothermic peaks on the DSC curves are shown in Fig. 6a, products have been completely crystallized in the four durations, as illustrated in Fig. 6b, but their crystallization phases were different according to Fig. 2, because the phase transitions require more time and thermal energy to be achieved. Furthermore, the crystallization velocity reached its maximum value in half of the time that was set as demonstrated in Fig. 6c.

Effect of 1-butanol as a dispersing agent on the crystallization process of the product is researched by employing 5 vol%, 15 vol%, 20 vol% or 40 vol% 1-butanol, 5 vol% deionized water, and EG (ethylene glycol) [31] at 200 °C for 24 h.

The exothermic peaks on DSC curves are shown in Fig. 7a that was different from Figs. 5(c2), 6(b), which previously required 200 °C to accomplish crystallization was advanced to at 160 °C when using 5 vol%, 15 vol%, or 20 vol% 1-butanol and to at 120 °C when hiring 40 vol% 1-butanol in Fig. 7b. Based on Figs. 5(c2), 6(b), the time needed for crystallization was 24 h, nevertheless, it was reduced to 20 h by adopting 5 vol%, 15 vol%, or 20 vol% 1-butanol and shortened to 15 h by choosing 40 vol% 1-butanol, as well as, corresponding the crest time was cut to 7.5 h or 12 h in Fig. 7c that demonstrated acceleration of crystalline rate is due to employing 1-butanol. It is inferred that 1-butanol has a lower mobile phase and polarity than deionized water; therefore, it can decrease the adhesive force of ions on the crystal nucleus, capillary force on the surface of nanoparticles, and the surface energy of crystallographic plane, leading to the nanoparticle requiring just minor energy to complete crystallization, also the nanoparticle growth and phase transition are hampered thereby the needed temperature and period are decreased and shortened. It is verified in Fig. 3 that precursors $In(OH)_3$ and InOOH are partially transformed into In_2O_3 and the width of the XRD diffraction peak is widened when the proportion of 1-butanol increased to 40 vol%.

4 Conclusions

Based on analysis on XRD patterns in Figs. 1, 2, 3, $In(OH)_3$ and InOOH are totally converted to In_2O_3, the preliminarily required solvothermal conditions are 200 °C, 24 h, 20 vol% 1-butanol content and 5 vol% deionized water content. On account of the limited number of experiments, this characterization method just gets approximate rection values, therefore, expect to acquire more accurate values requiring an extra quantity of synthetic works that will result in preparation period extension and cost increase. To address these issues, applying thermodynamic equations on the DSC curves to track the crystallization process for optimizing the correlated value is a preferable approach.

Depending on the method, the relevant reaction values can be effectively refined by analyzing the crystallinity and crystalline rate of IATO in diverse solvothermal conditions as demonstrated in Figs. 5, 6, 7 without extra experiments that heat and time can be, respectively, shortened from 200 to 160 °C and from 24 to 20 h, 1-butanol content can be reduced from 20 to 5 vol%.

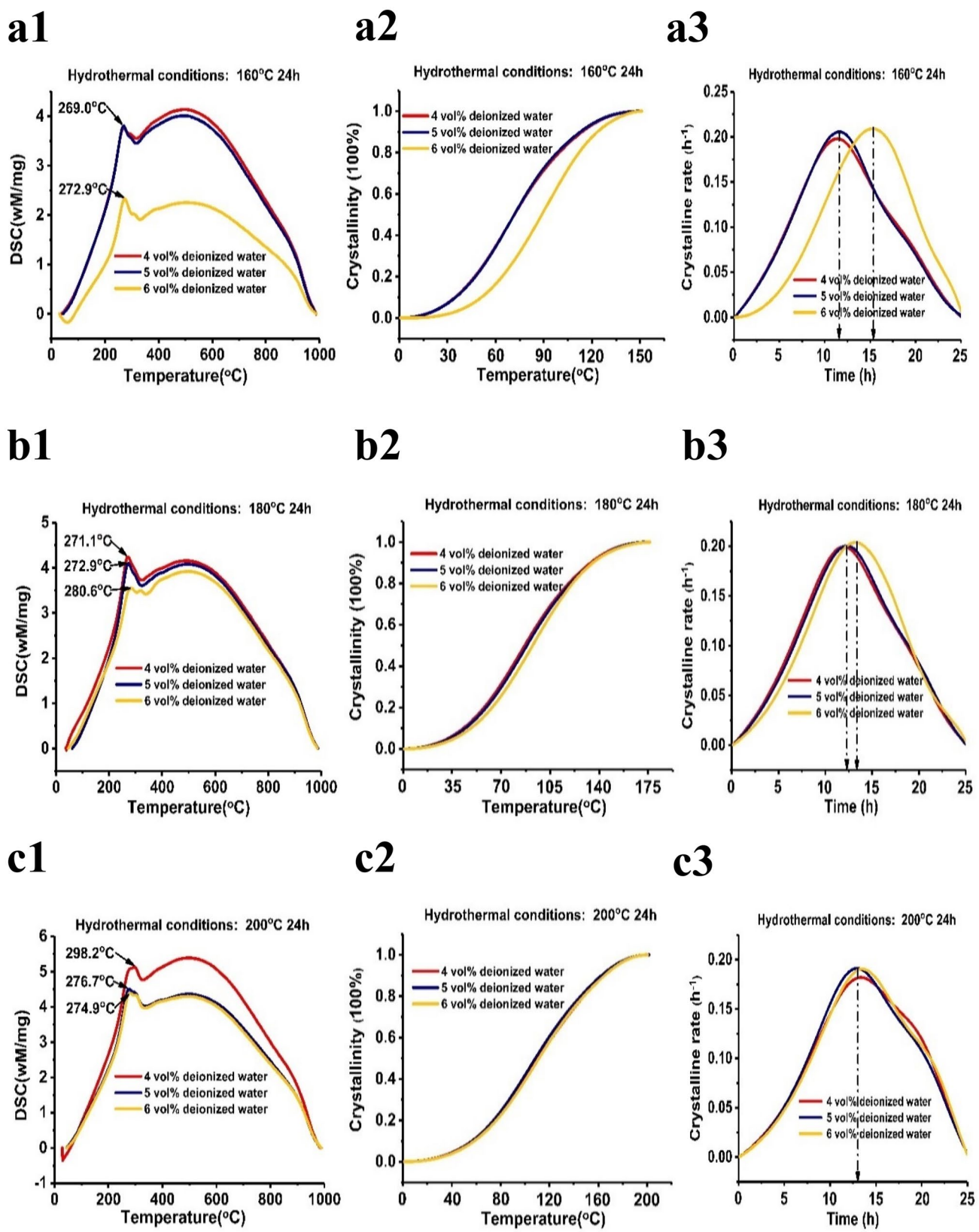

Fig. 5 DSC curve, crystallinity and crystallization rate of IATO nanoparticles synthesized at 160 °C, 180 °C or 200 °C for 24 h with using 4 vol%, 5 vol% or 6 vol% deionized water

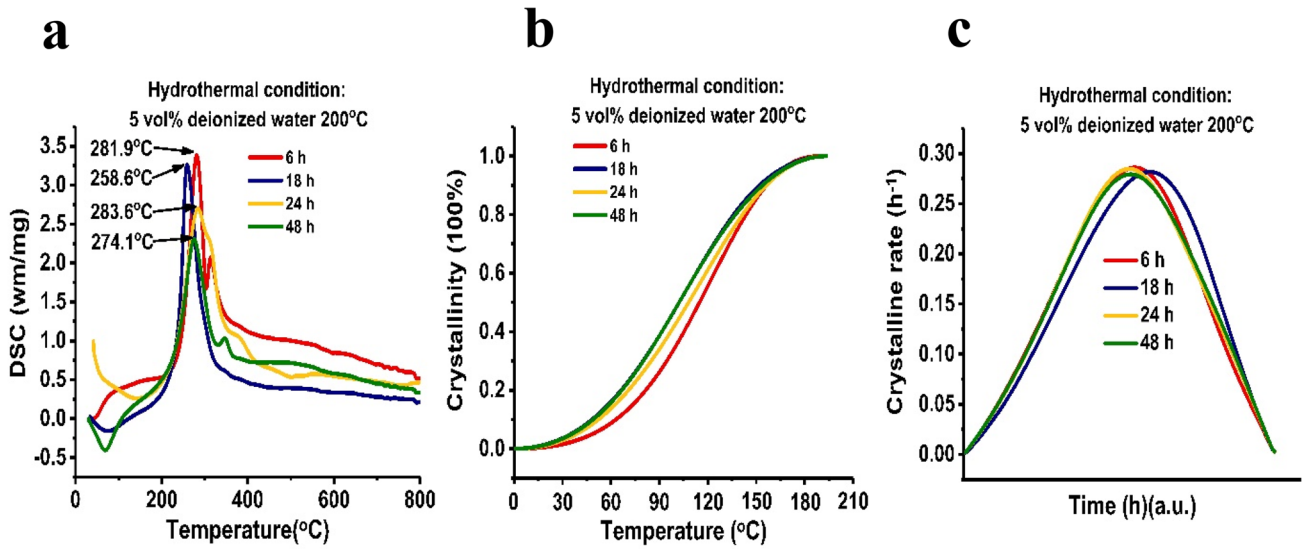

Fig. 6 DSC curve, crystallinity and crystallization rate of IATO nanoparticles synthesized at 200 °C with using 5 vol% deionized water for 24 h, 18 h, 24 h or 48 h

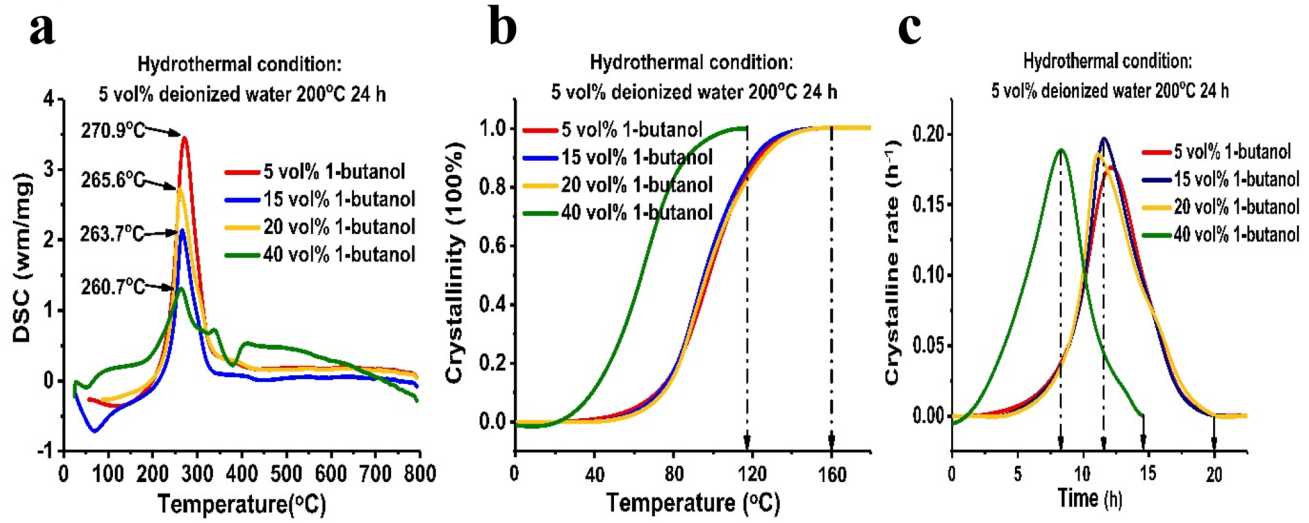

Fig. 7 DSC curve, crystallinity and crystallization rate of IATO nanoparticles synthesized at 200 for 24 h with using 5 vol% deionized water and diverse content of dispersing agent 1-butanol 5 vol%, 15 vol%, 20 vol% or 40 vol%

Acknowledgements This work is jointly supported by Yunnan Provincial Education Department Scientific Research Fund Project (KKJJ202107025); Kunming University of Science and Technology People Training Fund (KKZ3201907007); National Natural Science Foundation of China (11762009, 61865007); Key Program of Science and Technology of Yunnan Province (2019FA025) and The Yunnan Provincial Program for Foreign Talent (202105AO130015).

References

1. M. Cao, C. Hu, G. Peng, Y. Qi, E. Wang, Selected-control synthesis of PbO_2 and Pb_3O_4 single-crystalline nanorods. J. Am. Chem. Soc. **125**, 4982–4983 (2003)
2. Z.-R. Tang, Y. Zhang, Y.-J. Xu, A facile and high-yield approach to synthesize one-dimensional CeO_2 nanotubes with well-shaped hollow interior as a photocatalyst for degradation of toxic pollutants. RSC. Adv. **1**, 1772–1777 (2011)
3. Y. Teng, Y. Kusano, M. Azuma, M. Haruta, Y. Shimakawa, Morphology effects of Co_3O_4 nanocrystals catalyzing CO oxidation in a dry reactant gas stream. Catal. Sci. Technol. **1**, 920–922 (2011)

4. C. Chai, P. Peng, X. Wang, K. Li, Cuprous oxide microcrystals via solvothermal approach: morphology evolution and photocatalytic properties. Cryst. Res. Technol. **50**(4), 299–303 (2015)
5. X. Zhang, B. Li, C. Liu, Q. Chu, F. Liu, X. Wang, H. Chen, X. Liu, Rapid microwave-assisted solvothermal synthesis of morphology-tuned MnO_2 nanocrystals and their electrocatalytic activities for oxygen reduction. Mater. Res. Bull. **48**(7), 2696–2701 (2013)
6. B. Hecht, H. Bielefeldt, L. Novotny, Y. Inouye, D.W. Pohl, Local excitation, scattering, and interference of surface plasmons. Phys. Rev. Lett. **77**(9), 1889–1892 (1996)
7. K. Kneipp, Y. Wang, H. Kneipp, L.T. Perelman, I. Itzkan, R.R. Dasari, M.S. Feld, Single molecule detection using surface-enhanced raman scattering (SERS). Phys. Rev. Lett. **78**(9), 1667–1670 (1997)
8. C.L. Haynes, R.P.V. Duyne, Nanosphere lithography: a versatile nanofabrication tool for studies of size-dependent nanoparticle optics. J. Phys. Chem. B. **105**(24), 5599–5611 (2001)
9. D.A. Schultz, Plasmon resonant particles for biological detection. Curr. Opin. Biotechnol. **14**(1), 13–22 (2003)
10. S.I. Bozhevolnyi, V.S. Volkov, K. Leosson, Localization and waveguiding of surface plasmon polaritons in random nanostructures. Phys. Rev. Lett. **89**(18), 186801 (2002)
11. T. Kawano, H. Imai, Nanoscale morphological design of ZnO crystals grown in aqueous solutions. J. Ceram. Soc. Jpn. **118**(11), 969–976 (2010)
12. Y.J. Zhang, H. Ago, J. Liu, M. Yumura, K. Uchida, S. Ohshima, S. Iijima, J. Zhu, X.Z. Zhang, The synthesis of In, In_2O_3 nanowires and In_2O_3 nanoparticles with shape-controlled. J. Cryst. Growth. **264**, 363–368 (2004)
13. R.D.L. Rica, E. Bat, K.L. Herpoldt, H.N. Xie, S. Bertazzo, H.D. Maynard, M.M. Stevens, Nanoparticle growth via concentration gradients generated by enzyme nanopatterns. Adv. Func. Mater. **24**, 3692–3698 (2014)
14. Q. Jiang, M.D. Ward, Crystallization under nanoscale confinement. Chem. Soc. Rev. **43**, 2066–2079 (2014)
15. M. Shete, M. Kumar, D. Kim, N. Rangnekar, D.D. Xu, B. Topuz, K.V. Agrawal, E. Karapetrova, B. Stottrup, S. Al-Thabaiti, S. Basahel, K. Narasimharao, J.D. Rimer, M. Tsapatsis, Nanoscale control of homoepitaxial growth on a two-dimensional zeolite. Angew. Chem. Int. Ed. **56**, 535–539 (2017)
16. W.L. Barnes, A. Dereux, T.W. Ebbesen, Surface plasmon subwavelength optics. Nature **424**(6950), 824–830 (2003)
17. E. Hutter, J.H. Fendler, Exploitation of localized surface plasmon resonance. Adv. Mater. **16**(9), 1685–1706 (2004)
18. X.Y. Zhai, Y.Q. Zhang, Y.J. Chen, Y.Q. Ma, J.X. Liu, Controllable phase transition ITO nano powders and temperature-structure sensitivity. Chem. Phys. Lett. **742**, 137174 (2020)
19. Y.Q. Ma, X.Y. Zhai, J.X. Liu, Synthesis of hexagonal-phase indium tin oxide nanoparticles by deionized water and glycerol binary solvothermal method and their resistivity. J. Mater. Sci. **55**, 3860–3870 (2020)
20. I.G. Nielsen, S. Sommer, B.B. Iversen, Phase control for indium oxide nanoparticles. Nanoscale **13**, 4038 (2021)
21. W.H. Zhang, W.C. Zhang, B. Chen, R. Shao, R.F. Guan, W.D. Zhang, Q.F. Zhang, G.H. Hou, L. Yue, Controllable biomolecule-assisted synthesis and gas sensingproperties of In_2O_3 micro/nanostructures with double phases. Sens. Actuators. B. **239**, 270–278 (2017)
22. Y.J. Chen, X.Y. Zhai, J.X. Liu, One-step solvothermal synthesis of cubic ITO nanopowders. Rare. Metal. Mater. Eng. **48**(7), 2358–2363 (2019)
23. B.L. Yu, J.D. Jiang, *Practical thermal analysis* (Textile Industry Press, Bei Jing, 1990), pp. 135–187
24. K. Matusita, S. Sakka, Y. Matsui, Determination of the activation energy for crystal growth by differential thermal analysis. J. Mater. Sci. **10**, 961–966 (1975)
25. T.M. Aper, F.K. Yam, K.P. Beh, Influence of temperature and nickel catalyst on the structural and optical properties of indium oxide nanostructured films synthesized by chemical vapor deposition technique. Mater. Sci. Semicond. Process. **132**, 105925 (2021)
26. A.K. Isiyaku, A.H. Ali, S.G. Abdu, M. Tahan, N.A. Raship, A.S. Bakri, N. Nayan, Improvement of transparent conductive indium tin oxide based multilayer films on p-silicon through the inclusion of thin copper-aluminium metals interlayer. Thin. Solid. Films. **738**, 138959 (2021)
27. J.H. Lee, J.Z. Sheng, H. An, T.H. Hong, H.Y. Kim, H.K. Lee, J.H. Seok, J.W. Park, J.H. Lim, J.S. Park, Metastable rhombohedral phase transition of semiconducting indium oxide controlled by thermal atomic layer deposition. Chem. Mater. **32**(17), 7397–7403 (2020)
28. S. Zhang, P. Song, Z.X. Yang, Q. Wang, Facile hydrothermal synthesis of mesoporous In_2O_3 nanoparticles with superior formaldehyde-sensing properties. Phys. E: Low-dimens. Syst. Nanostructures. **97**, 38–44 (2018)
29. S.A. Palomares-Sancheza, B.E. Watts, D. Klimm, A. Baraldi, A. Parisini, S. Vantaggio, R. Fornari, Sol-gel growth and characterization of In_2O_3 thin films. Thin. Solid. Films. **645**, 83–390 (2018)
30. S. Tsukuda, H. Uesugi, M. Kita, T. Omata, Formation of spherical, rod- and branch-shaped colloidal In_2O_3 nanocrystals through simple thermolysis of an oleate precursor. Mater. Trans. **61**(3), 462–468 (2020)
31. R. Sarhaddi, N. Shahtahmasebi, M.R. Rokn-Abadi, M.M. Bagheri-Mohagheghi, Effect of post-annealing temperature on nano-structure and energy band gap of indium tin oxide (ITO) nano-particles synthesized by polymerizing–complexing sol–gel method. Phys. E. **43**(1), 452–457 (2010)